ISSN 0036-0236, Russian Journal of Inorganic Chemistry, 2024. © Pleiades Publishing, Ltd., 2024.

COORDINATION COMPOUNDS

Coordination of Manganese(III) Porphyrins with Pyridine as a Model of Formation of Donor–Acceptor Dyads with Fullerene Acceptors

E. N. Ovchenkova[a], *, A. A. Elkhovikova[b], and T. N. Lomova[a]

[a] *Krestov Institute of Solution Chemistry, Russian Academy of Sciences, Ivanovo, 153045 Russia*

[b] *Ivanovo State University of Chemical Technology, Ivanovo, 153000 Russia*

**e-mail: enk@isc-ras.ru*

Received July 6, 2023; revised August 8, 2023; accepted September 6, 2023

Abstract—The coordination of pyridine molecules with tetrapyrrole macrocyclic complexes of manganese(III) was studied depending on the ligand structure. The coordination in toluene was ended in all cases in the formation of 1 : 1 complexes, the structure of which was established using MALDI-TOF mass spectrometry and ^{1}H NMR spectroscopy. The numerical values of the stability constants of the coordination complexes were found to vary from 0.16 to 10^4 L/mol, depending on the nature of the axial anion in the manganese(III) complex, the structure of the tetrapyrrole macrocycle, and the functional substitution in the macrocycle. The data obtained are useful for selecting the structures in the design of metal porphyrin-based hybrid materials by the immobilization and supramolecular chemistry methods.

Keywords: manganese(III) porphyrins, organic base, donor–acceptor complexation, spectral properties, stability

DOI: 10.1134/S0036023623602726

INTRODUCTION

Among the great diversity of metal porphyrins (MPs), manganese complexes occupy a prominent place in the chemistry of macroheterocyclic compounds. Being predominantly in a high-spin state, manganese in the structure of the porphyrin complex can have several oxidation states (+2, +3, +4 or +5), which is reflected in spectral, electrochemical, and coordination properties. The interest in the study of manganese porphyrin complexes (MnPs) is associated with the possibility of their practical application as catalysts for oxidation of various organic compounds [1–4]. Particular attention is given to the use of MnPs in medicine as mimetic enzymes [5, 6], contrast agents for high-relaxation magnetic resonance imaging [7], photosensitizers in photodynamic inactivation of pathogenic microorganisms [8, 9], and as radio- and chemosensitizers in the treatment of tumor diseases [10, 11].

The design of MP-based donor–acceptor systems with N-heterocyclic bases, bioligands, fullerenes, and graphene is a promising approach to the simulation of practically valuable processes. Numerous studies are addressed to the donor–acceptor systems based on zinc porphyrin complexes [12–19]. However, increasing attention of researchers is also attracted by porphyrin complexes with other metal ions [20–24], including manganese [2, 3, 25–27]. For example, (chloro)(5,10,15,20-tetraphenylporphynato)manganese(III) was covalently attached to the graphene oxide surface (GO) [28]. The complex was characterized using spectroscopic techniques and scanning and transmission electron microscopy. Under UV irradiation, the complex has displayed high stability fast photoinduced electron transfer (PET) from the photoexcited porphyrin moiety to GO layers, and high photocatalytic characteristics in water reduction to give hydrogen [28].

The synthesis and crystal/molecular structures of new manganese(III) porphyrin complexes with imidazole, piperidine, pyridine, and 1,4-diazabicyclo [2, 2, 2]octane were reported in [29]. The axial coordination of N-bases with MPs is studied for in vivo modeling of processes involving metal-containing enzymes and catalytic properties of the MP reaction centers [30]. The donor–acceptor assembly through the axial coordination is relatively simply implemented and allows you to create systems close to natural.

We have here studied manganese complexes MnPs axially bounded with the acetate ions where P is 5,10,15,20-tetraphenylporphin (AcO)MnTPP, 5,10,15,20-(tetra-4-*tert*-butylphenyl)porphin (AcO)MnT^tBuPP, and octakis(4-*tert*-butylphenyl)tetraazaporphin (AcO)MnTAP(4-^{t}BuPh)$_8$ (Fig. 1). Quantitative parameters were found and the stoichiometric mechanism of their reactions with pyridine (Py) was substantiated; spectroscopic characteritics and stability constants (K) were determined; and correlations between the quantitative characteristics and chemical structure of pyridine complexes were revealed resorting to the available

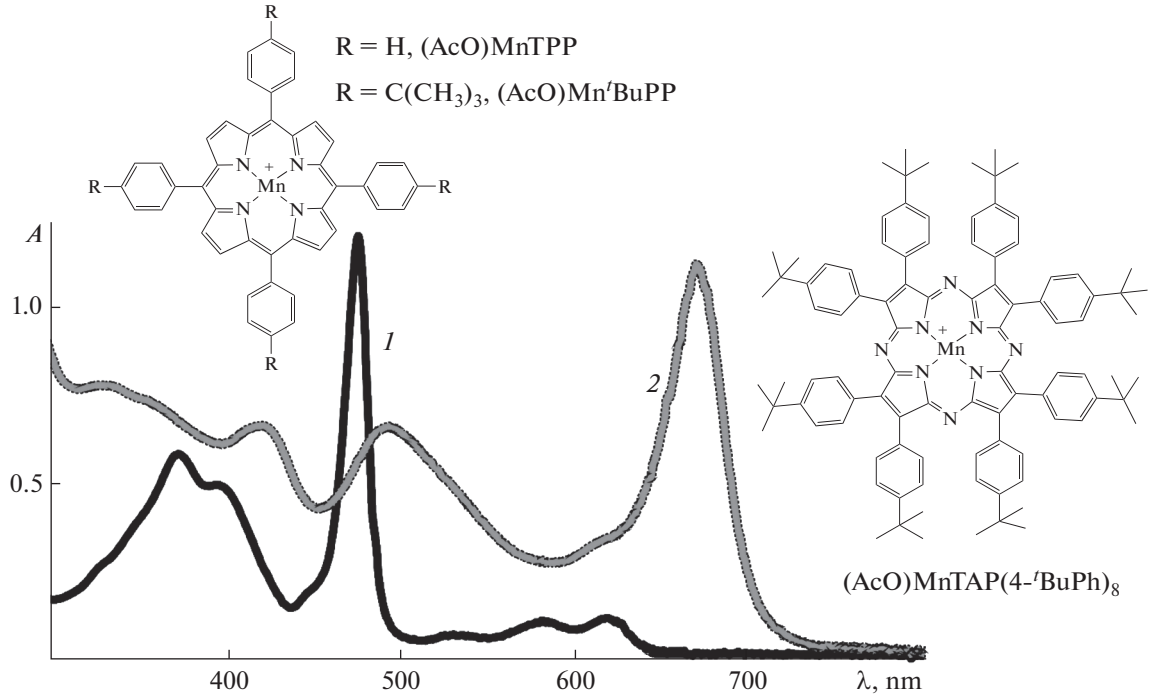

Fig. 1. Structural formulas and the UV-vis spectra of (*1*) (AcO)MnTPP/(AcO)MnT^{t}BuPP and (*2*) (AcO)MnTAP(4-^{t}BuPh)$_8$ in toluene.

published data on similar compounds. Since the pyridyl group is used as a bridge in the coordination of metal porphyrins with fullerene acceptors for the design of photoinduced charge separation donor–acceptor systems, a relevant task is to study the coordination involving the unsubstituted pyridine molecules and to establish the chemical structure, spectral properties, and stability of the resulting complexes.

EXPERIMENTAL

(AcO)MnTPP and (AcO)MnT^{t}BuPP were prepared by the reaction of $Mn(AcO)_2{\cdot}4H_2O$ with a specified porphyrin in refluxing dimethylformamide [31]. (AcO)MnTAP(4-^{t}BuPh)$_8$ was obtained by template cyclotetramerization of bis(4-*tert*-butylphenyl)fumaronitrile with manganese(II) acetate in 2-dimethylaminoethanol at 150°C [32]. The product identification and purity control were performed using UV-vis and IR spectra and MALDI-TOF mass spectra.

(AcO)MnT^{t}BuPP. UV-vis, toluene (λ_{max}, nm (logε)): 375 (4.78), 399 (4.71), 478 (5.10), 589 (3.99), 627 (4.13). IR (KBr), ν, cm^{-1}: 2962, 2904 $\nu_{as}(CH_3)$; 2867 $\nu_s(CH_3)$; 1631 ν_{as}(O–C–O); 1535, 1499 ν(C=C)$_{Ph}$; 1462 ν(C=N); 1396, 1364 δ(^{t}Bu); 1342 ν_s(O–C–O); 1267, 1204 δ(^{t}Bu); 1109, 1074, 1008 δ(C–H)$_{Ph}$; 853, 814 δ(C–H)$_{Pyr}$; 803, 744 γ(C$_\beta$–C); 716, 658, 640 γ(C–H)$_{Ph}$. IR (CsBr), ν, cm^{-1}: 586, 567, 474, 449, 408 γ(C–H)$_{Ph}$; 306 ν(Mn–N). MS (MALDI-TOF): *m/z* 892.33 [M–AcO]$^+$ (calcd. for $C_{60}H_{60}MnN_4$ 892.11). ^{1}H NMR ($CDCl_3$), δ, ppm: 8.35 (br.s, $H_{o,m}$), 1.62 (s, H^{t}_{Bu}), 1.33 (s, H_{AcO}), –22.58 (br.s, H_β).

(AcO)MnTPP. UV-vis, toluene (λ_{max}, nm (logε)): 373 (4.62), 395 (4.55), 477 (4.94), 586 (3.86), 621 (3.90). IR (KBr), ν, cm^{-1}: 1625 ν_{as}(O–C–O); 1596, 1488 ν(C=C)$_{Ph}$; 1440 ν(C=N); 1344 ν_s(O–C–O); 1298, 1232 ν(C–H)$_{Pyr}$; 1204, 1180, 1160, 1076 δ(C–H)$_{Ph}$; 1012 δ(C–H)$_{Pyr}$; 804, 744 γ(C$_\beta$–C); 716, 704, 664, 621 γ(C–H)$_{Ph}$. IR (CsBr), ν, cm^{-1}: 566, 521, 454, 411, 367 γ(C–H)$_{Ph}$; 295 ν(Mn–N). MS (MALDI-TOF): *m/z* 668.02 [M–AcO]$^+$ (calcd. for $C_{44}H_{28}MnN_4$ 667.68). ^{1}H NMR ($CDCl_3$), δ, ppm: 8.28 (br.s, $H_{o,m}$), 1.34 (s, H_{AcO}), –22.78 (br.s, H_β).

(AcO)MnTAP(4-^{t}BuPh)$_8$. UV-vis, toluene (λ_{max}, nm (logε)): 421 (4.51), 494 (4.50), 619 (sh), 673 (4.74). IR (KBr), ν, cm^{-1}: 2962, 2905, 2868, 1717, 1609, 1477, 1463, 1384, 1364, 1299, 1269, 1197, 1147, 1109, 997, 891, 850, 839, 811, 751, 635, 599, 585, 563. IR (CsBr), ν, cm^{-1}: 508, 479, 406, 362, 299. MS (MALDI-TOF): *m/z* 1425.47 [M–AcO]$^+$ (calculated for $C_{96}H_{104}N_8Mn$ 1424.87). The ^{1}H NMR spectrum was reported previously [33].

Pyridine (analytical grade) and toluene were dried by potassium hydroxide and distilled prior to use (bp = 110.6 and 115.3°C for Py and toluene, respectively).

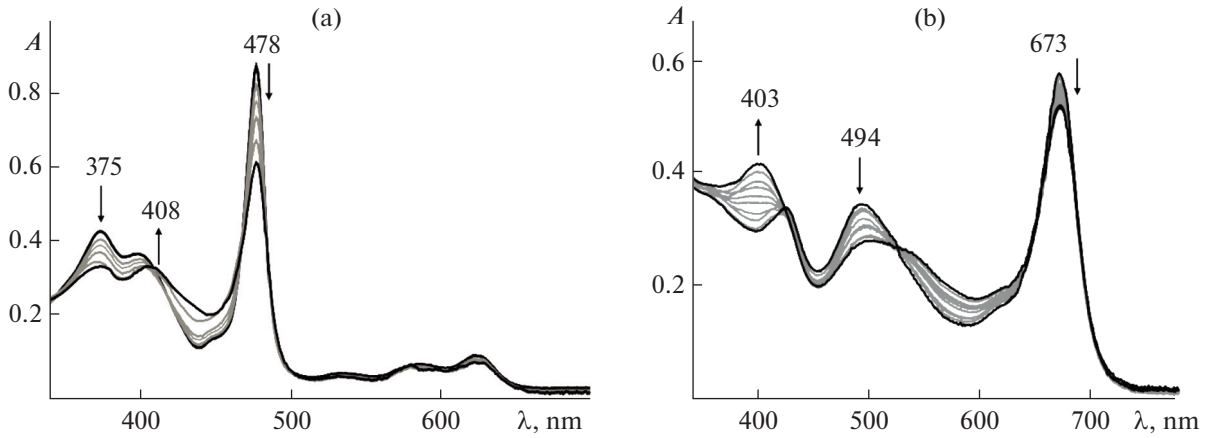

Fig. 2. Change in the UV-vis spectra of (a) (AcO)MnT^{t}BuPP and (b) (AcO)MnTAP(4-^{t}BuPh)$_8$ in toluene with 0 to 10 mol/L of Py added.

The reaction of MnP with Py was spectrophotometrically studied in toluene at 298 K by the method of molar ratios at constant MP concentrations of 7.0×10^{-6} and 1.4×10^{-5} mol/L for (AcO)MnT^{t}BuPP, (AcO)MnTPP, and (AcO)MnTAP(4-^{t}BuPh)$_8$, respectively, and Py concentrations varying from 0 to 10 mol/L.

The equilibrium constants (K) were found from equation (1) using the least-squares method:

$$K = \frac{(A_i - A_0)/(A_\infty - A_0)}{1-(A_i - A_0)/(A_\infty - A_0)} \times \frac{1}{\left(\left(C^0_{Py} - C^0_{MnP}(A_i - A_0)/(A_\infty - A_0)\right)^n\right)}, \quad (1)$$

where C^0_{Py} and C^0_{MnP} is the initial concentration of Py and MnP in toluene, respectively; A_0, A_i, A_∞ is absorbance at the working wavelengths for MnP, equilibrium mixture at a definite Py concentration, and the reaction product, respectively. The relative error in the determination of K did not exceed 15%. The stoichiometric coefficient for Py (n) was defined as a slope of the straight line $\log I_i = f(\log C_{Py})$, where I_i is the "indicator" ratio defined as $I_i = A_i - A_0/A_\infty - A_i$.

UV-vis, IR, ^{1}H NMR, and MALDI-TOF mass spectra were measured using a UV-vis Agilent 8453 spectrophotometer, VERTEX 80v and Bruker Avance III-500 spectrometers, and Shimadzu Confidence mass spectrometer, respectively.

RESULTS AND DISCUSSION

The UV-vis spectra of MnPs synthesized correspond to the hyper type due to the presence of additional intense absorption bands extra to the normal type spectra [34]. The UV-vis spectra of (AcO)MnTPP in toluene exhibit the intense charge transfer band at 477 nm and two less intense bands for $\pi \rightarrow \pi^*$ transitions in the visible region at 586 and 621 nm (Q band). The appearance of four electron-donating *tert*-butyl groups in (AcO)MnT^{t}BuPP practically does not change the position of the charge transfer band, whereas the Q-bands are markedly red-shifted. The red shift of the Q-band and the sharp increase in the band intensity in the spectrum of (AcO)MnTAP(4-^{t}BuPh)$_8$ take place, since the absorption bands for the electronic transitions of porphyrin complexes in the visible region are no longer quasi-forbidden after aza substitution in the macrocycle [35].

In all three cases, bonding of Py molecules to manganese(III) complex is accompanied by displacements and intensity changes of the main absorption bands of the chromophore, with the isosbestic points being preserved. As increasing volumes of Py are added to the (AcO)MnTtBuPP toluene solution, the intensity of spectral bands at 478 nm and 375 nm gradually decreases and the band at 399 nm shifts to 408 nm (Fig. 2a). Similar spectral changes also take place for (AcO)MnTPP. In the case of (AcO)MnTAP(4-^{t}BuPh)$_8$, bonding of the pyridine molecule is also accompanied by the decrease in the intensity of bands at 673 nm and 494 nm, but the maximum at 421 nm (B-band) is blue-shifted to 403 nm (Fig. 2b). The spectrum of the reaction product for the three complexes studied still belongs to the macrocyclic chromophore of the manganese(III) complex. The reversibility of the above spectral changes was demonstrated experimentally, that is, by dilution of reaction mixtures with respect to Py, which means that the reaction has proceeded to equilibrium.

The 1 : 1 stoichiometric composition of MnP complexes with Py can be determined from the data of Fig. 3 (Experimental). Slow irreversible reactions of displacement of the axial acetate ion were not detected in the experiment, while the spectral changes caused by the reaction (directions of band shifts) attest to a decrease in the deviation of the central Mn atom from the porphyrin plane [26]. It was from this concluded

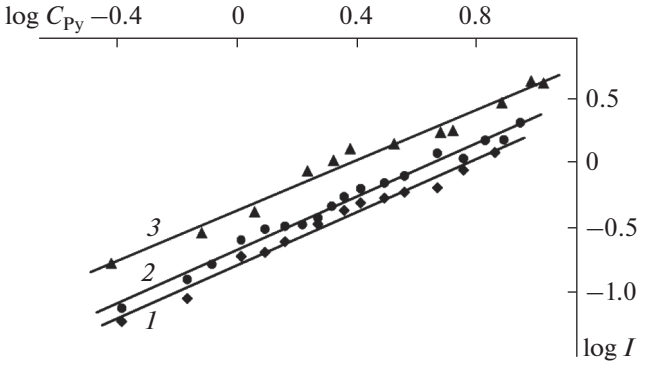

Fig. 3. Plot of log$I$ vs. logC_{Py} for the reaction of (*1*) (AcO)MnTPP (tanα = 1.03, R^2 = 0.98), (*2*) (AcO)MnT^{t}BuPP (tanα = 1.03, R^2 = 0.98), and (*3*) (AcO)MnTAP(4-^{t}BuPh)$_8$ (tanα = 0.96, R^2 = 0.99) with Py in toluene at 298 K.

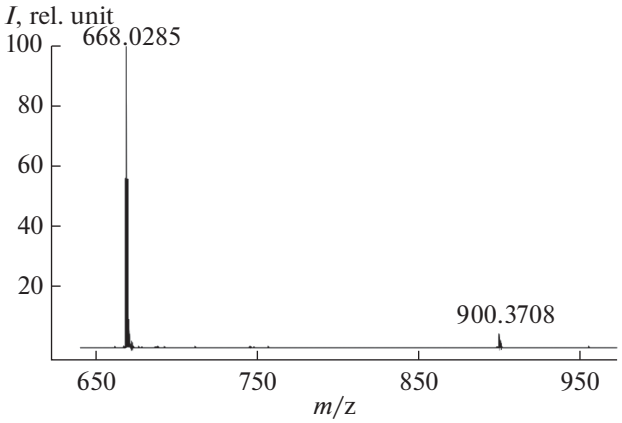

Fig. 4. MALDI-TOF mass spectum of (AcO)(Py)MnTPP.

that Py and AcO^- occupy *trans*-positions relative to the plane of the equatorial macrocyclic ligand.

The formation of coordination complexes with Py was confirmed by the MALDI-TOF mass spectrometry data. The mass spectra of MnPs are the single intense line corresponding to the $[M–AcO]^+$ complex ion formed upon elimination of the acetate ligand (see Experimental). The mass spectrometric analysis of the donor–acceptor complexes with Py carried out using 2,5-dihydroxybenzoic acid (DHB) matrix has shown the presence of the low-intensity signals of the complexes along with the signals of free MnPs. Figure 4 represents the MALDI-TOF mass spectrum of (AcO)(Py)MnTPP with peaks corresponding to $[M–AcO]^+$ (*m*/z 668.03) and $[M–AcO + Py + DHB]^+$ (*m*/z 900.37). In the case of (AcO)MnT^{t}BuPP and (AcO)MnTAP(4-^{t}BuPh)$_8$, the $[M–AcO]^+$ and $[M–AcO + Py + DHB]^+$ signals with *m*/z 892.35/1425.47 and 1124.21/1657.82, respectively, were also present.

Manganese(III)porphyrins in which the central metal atom occurs in the $3d^4$ configuration are paramagnetic; therefore, their ^{1}H NMR signals are shifted and broadened with respect to the spectral signals of diamagnetic complexes [36–38]. The signals of pyrrole proton (H_β) and *meta*-/*ortho*-protons of the phenyl groups ($H_{m,o}$) in the spectrum of (AcO)MnTPP in $CDCl_3$ are manifested as broadened singlets at −22.78 ppm and 8.28 ppm, respectively. No signals for the phenyl *para*-protons are detected in the spectrum. According to published data [36], they are located at 7.3 ppm (in CD_2Cl_2) and, in our cases, they are superimposed by the signal of $CDCl_3$. The introduction of *tert*-butyl groups at the periphery of the macrocycle induces downfield shifts of the H_β and $H_{m,o}$ signals of (AcO)MnT^{t}BuPP by 0.2 ppm and 0.07 ppm, respectively (Fig. 5a). The *tert*-butyl and acetate CH_3 protons resonate in the ^{1}H NMR spectrum of (AcO)MnT^{t}BuPP at 1.62 ppm and 1.3 ppm, respectively. The ^{1}H NMR spectrum of (AcO)MnTAP(4-^{t}BuPh)$_8$ was reported previously [33]. The introduction of the Py molecule into the MnP gives rise to new proton signals for the pyridine ring at 8–7 ppm (Fig. 5b), which are shifted downfield with respect to the signals of uncoordinated pyridine [39]. The formation of the Py → Mn donor–acceptor bond also induces a shift of the macrocycle proton signals. For example, the $H_{m,o}$ signals in the H^1 NMR spectrum of (AcO)(Py)MnT^{t}BuPP, shift downfield by 1.15 ppm, whereas the H_β signals shift upfield by 0.2 ppm. (Fig. 5b). Analogical changes take place for other MnPs studied in this work and reported in the literature [37, 40]. This upfield shift of the β-proton signals was attributed [37] to the change in the orbital symmetry of the manganese atom upon the deformation of the porphyrin macrocycle caused by axial coordination.

The stability constants of the MnP coordination complexes with Py (Table 1) vary depending on the chemical structure of the macrocycle and the nature of the anionic axial ligand within four orders of magnitude.

A sharp increase in the *K* value takes place for the manganese(III) complex with the anionic weak-field axial ligand, $(OClO_3)$MnTPP, for which the Chernyaev's *trans*-effect induces strong bonding of the *trans*-ligand Py. Moderate *K* values of approximately the same order of magnitude were found for the other manganese(III) complexes (Table 1).

The change in the nature of the macrocycle has the noticeable effect on the stability of the complexes with Py. As can be seen from Table 1, (AcO)(Py)MnOEP is most stable among the complexes with the acetate ligand. In general, β-alkyl substituents increase the *K* value compared to phenyl substituents in the *meso*-positions. Indeed, (AcO)(Py)MnOEP is 5 times more stable than (AcO)(Py)MnTPP. The tetra-aza substitution in the macrocycle has a less pronounced effect. The stability constants of (AcO)(Py)MnTAP(4-^{t}BuPh)$_8$ and

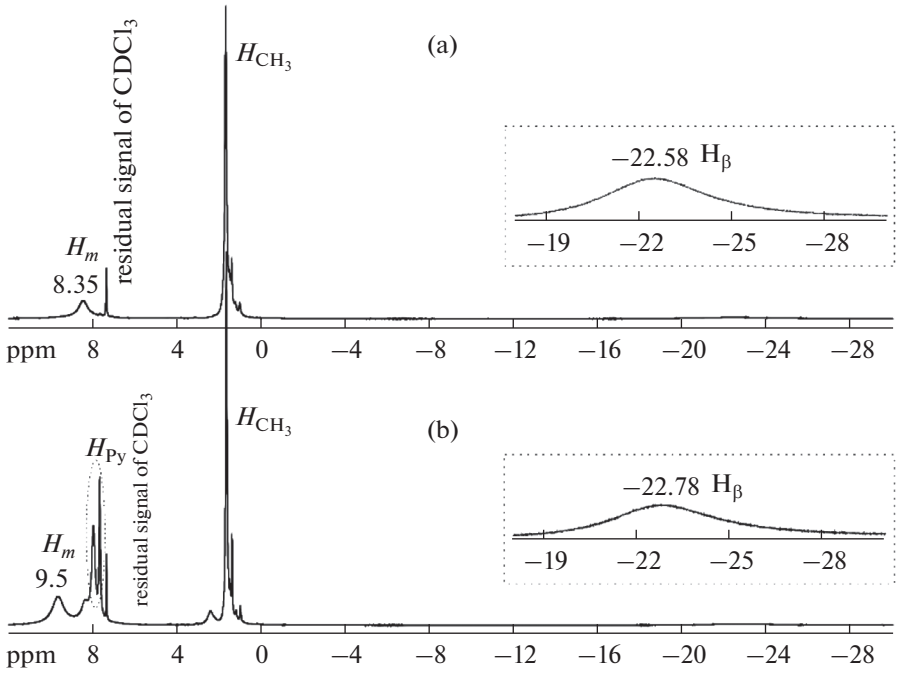

Fig. 5. ^{1}H NMR spectra of (a) (AcO)MnT^{t}BuPP and (b) (AcO)(Py)MnT^{t}BuPP in $CDCl_3$.

Table 1. Stability constants of the 1 : 1 coordination complexes of MPs with Py in toluene at 298 K

Coordination complex	K, L/mol
(AcO)(Py)MnTPP	0.16 ± 0.02
(AcO)(Py)MnT^{t}BuPP	0.22 ± 0.03
(AcO)(Py)MnTAP(4-^{t}BuPh)$_8$	0.38 ± 0.05
(AcO)(Py)MnOEP* [26]	0.85 ± 0.06
(AcO)(Py)MnTMT^{t}BuP* [26]	0.33 ± 0.02
(AcO)(Py)MnPc(3,5-^{t}BuPhO)$_8$* [43]	0.30 ± 0.04
(Cl)(Py)MnTPP [42]	1.34
($OClO_3$)(Py)MnTPP [42]	1.20×10^4
(AcO)(Py)CrTPP [42]	4.0×10^2
[O=Mo(Py)TPP]$^+$ OH^- [42]	9.14×10^3
O=W(OH)(Py)TPP [42]	1.33×10^4
(X)(Py)AlTPP, X = Cl, OH, AcO, Acac [44]	65–1.33×10^2 **
(Cl)(Py)InTPP [42]	9.45×10^2
(Cl)(Py)FeTPP [42]	4.79×10^3
$(Cl)_2$(Py)ZrTPP [42]	3.65×10^4
$(Cl)_2$(Py)HfTPP [42]	1.50×10^4
(Py)CoTPP [45]	7.94×10^2 ***
(Py)CoT(*p*-OCH_3)PP [46]	4.85×10^2
(Py)CoT(CN)PP [47]	1.58×10^4
(Py)Co(2-Py)P * [48]	3.56×10^2

* OEP is the 2,3,7,8,12,13,17,18-octaethylporphin dianion, TMTBP is the 3,7,12,18-tetramethyl-2,8,13,17-tetra(*n*-butyl)porphin dianion, Pc(3,5-^{t}BuPhO)$_8$ is the octakis(3,5-di-*tert*-butylphenoxy)phthalocyanine dianion, (2-Py)P is the 3,7,8,12,18-hexamethyl-13,17-diethyl-5-(2-pyridyl)porphin dianion.
** In $CHCl_3$.
*** In CH_2Cl_2.

(AcO)(Py)MnPc(3,5-^{t}BuPhO)$_8$ are comparable to within the error of determination and are ~2 and 1.5–2 times lower than the K values for (AcO)(Py)MnOEP and (AcO)(Py)MnTPP, (AcO)(Py)MnT^{t}BuPP, respectively. Perhaps, this is due to the decrease in the size of the coordination cavity of the porphyrin macrocycle compared to phthalocyanine and to the presence of electron-withdrawing nitrogen atoms at the *meso*-positions [41].

As can be seen from a comparison of the stability of MP–pyridine complexes with various metal cations (Table 1), manganese(III) complexes are the least stable. This provides the unique opportunity to verify how the strength of axial fullerene electron acceptor bonding through the pyridyl group affects the charge separation efficiency in the excited state by studying the PET phenomenon in MP-based donor–acceptor systems. It can be seen from the example of the donor–acceptor coordination systems based on MP donors and pyridyl-substituted fullero[60]pyrrolidine acceptors studied previously [42], that the manganese-containing systems have also lower stability compared to the analogical cobalt(II)-based systems, while demonstrating higher photoconversion performance characteristics: photocurrent density (j_{ph}^{avg}, $\mu A/cm^2$) and the differential incident photon-to-current efficiency ($IPCE^{365\ nm}$, %) in the Ti|photoactive film|0.5 mol/L Na_2SO_4|Pt short-circuited electrochemical cell. Since data of this type are poorly addressed in the literature, one may hope that the results of this study would stimulate further research along this line.

CONCLUSION

Data on the equilibrium constants, stoichiometry, and key spectral properties (UV-vis and ^{1}H NMR spectroscopy and mass spectrometry) of the donor–acceptor complexes of MnPs with Py are presented. The relationship between the stability of the obtained coordination complexes and their molecular structure is analyzed and characteristic features of manganese(III) porphyrin complexes are shown in comparison with analogs with another central ion, which open new prospects in the study of MP-based donor-acceptor systems with PET properties.

ACKNOWLEDGMENTS

Performed using the research equipment of the Center for Collective Use "Upper Volga Regional Center for Physicochemical Research."

FUNDING

This study was supported by the Russian Science Foundation (grant no. 21-73-20090).

CONFLICT OF INTEREST

The authors of this work declare that they have no conflicts of interest.

REFERENCES

1. A. M. Meireles, A. S. Guimarães, G. R. Querino, et al., Appl. Organomet. Chem. **35** (2021). https://doi.org/10.1002/aoc.6400
2. F. Gou, Q. Bian, H. Pan, et al., J. Mol. Struct. **1281**, 135116 (2023). https://doi.org/10.1016/j.molstruc.2023.135116
3. M. Jokazi, L. S. Mpeta, and T. Nyokong, J. Electroanal. Chem. **901**, 115748 (2021). https://doi.org/10.1016/j.jelechem.2021.115748
4. T. Lomova, Y. Tsaplev, M. Klyueva, et al., J. Organomet. Chem. **945**, 121880 (2021). https://doi.org/10.1016/j.jorganchem.2021.121880
5. A. Žiniauskaitė, S. Ragauskas, A. K. Ghosh, et al., Ocul. Surf. **17**, 257 (2019). https://doi.org/10.1016/j.jtos.2019.02.006
6. Y. Zheng, Y. Yuan, Y. Chai, et al., Biosens. Bioelectron. **66**, 585 (2015). https://doi.org/10.1016/j.bios.2014.12.022
7. H.-S. Lu, M.-Y. Wang, F.-P. Ying, et al., Bioorg. Med. Chem. **35**, 116090 (2021). https://doi.org/10.1016/j.bmc.2021.116090
8. G. Karimipour, S. Kowkabi, and A. Naghiha, Braz. Arch. Biol. Technol. **58**, 431 (2015). https://doi.org/10.1590/S1516-8913201500024
9. K. G. Yu, D. H. Li, C. H. Zhou, et al., Chine. Chem. Lett. **20**, 411 (2009). https://doi.org/10.1016/j.cclet.2008.11.030
10. K. A. Ashcraft, M.-K. Boss, A. Tovmasyan, et al., Int. J. Radiat. Oncol. Biol. Phys **93**, 892 (2015). https://doi.org/10.1016/j.ijrobp.2015.07.2283
11. D. H. Weitzel, A. Tovmasyan, K. A. Ashcraft, et al., Mol. Cancer Ther. **14**, 70 (2015). https://doi.org/10.1158/1535-7163.MCT-14-0343
12. A. V. Ezhov, A. E. Aleksandrov, K. A. Zhdanova, et al., Synth. Met. **269**, 116567 (2020). https://doi.org/10.1016/j.synthmet.2020.116567
13. B. Fu, Y. Che, X. Yuan, et al., Dyes Pigm. **196**, 109754 (2021). https://doi.org/10.1016/j.dyepig.2021.109754
14. E. Gacka, G. Burdzinski, B. Marciniak, et al., Phys. Chem. Chem. Phys. **22**, 13456 (2020). https://doi.org/10.1039/D0CP02545C
15. A. S. Malyasova, P. N. Smirnova, and O. I. Koifman, Russ. J. Inorg. Chem. **67**, 388 (2022). https://doi.org/10.1134/S0036023622030093
16. R. Chitta, D. Badgurjar, G. Reddy, et al., J. Porphyrins Phthalocyanines **25**, 469 (2021). https://doi.org/10.1142/S1088424621500395
17. J. Janczak, Polyhedron **178**, 114313 (2020). https://doi.org/10.1016/j.poly.2019.114313
18. Y. Li, G. Wang, X. Feng, et al., J. Mol. Struct. **1242**, 130819 (2021). https://doi.org/10.1016/j.molstruc.2021.130819

19. L. C. Nene, M. E. Managa, D. O. Oluwole, et al., Inorg. Chim. Acta **488**, 304 (2019). https://doi.org/10.1016/j.ica.2019.01.012
20. A. Amati, P. Cavigli, A. Kahnt, et al., J. Phys. Chem. A **121**, 4242 (2017). https://doi.org/10.1021/acs.jpca.7b02973
21. N. Amiri, F. B. Taheur, S. Chevreux, et al., Tetrahedron **73**, 7011 (2017). https://doi.org/10.1016/j.tet.2017.10.029
22. N. G. Bichan, E. N. Ovchenkova, A. A. Ksenofontov, et al., J. Mol. Liq. **326**, 115306 (2021). https://doi.org/10.1016/j.molliq.2021.115306
23. K. P. Birin, I. A. Abdulaeva, D. A. Polivanovskaya, et al., Russ. J. Inorg. Chem. **66**, 193 (2021). https://doi.org/10.1134/S0036023621020029
24. S. A. Znoiko, T. V. Kustova, E. I. Pavlova, et al., Russ. J. Gen. Chem. **91**, 190 (2021). https://doi.org/10.1134/S1070363221020067
25. E. N. Ovchenkova, N. G. Bichan, N. O. Kudryakova, et al., Dyes Pigm. **153**, 225 (2018). https://doi.org/10.1016/j.dyepig.2018.02.023
26. E. N. Ovchenkova, M. E. Klyueva, and T. N. Lomova, Russ. J. Inorg. Chem. **62**, 1483 (2017). https://doi.org/10.1134/S0036023617110134
27. H. Wang, Z. Fan, T. Cao, et al., J. Alloys Compd. **887**, 161462 (2021). https://doi.org/10.1016/j.jallcom.2021.161462
28. X. Li, K. Li, D. Wang, et al., J. Porphyrins Phthalocyanines **21**, 179 (2017). https://doi.org/10.1142/S1088424616501236
29. N. Lahanas, P. Kucheryavy, R. A. Lalancette, et al., Acta Crystallogr., Sect. C **75**, 304 (2019). . https://doi.org/10.1107/S2053229619001232
30. K. Kadish, K. Smith, and R. Guilard, *The Porphyrin Handbook*, vol. 4 (Academic Press, New York, 1999).
31. A. D. Adler, F. R. Longo, F. Kampas, et al., J. Inorg. Nucl. Chem. **32**, 2443 (1970). https://doi.org/10.1016/0022-1902(70)80535-8
32. E. N. Ovchenkova, M. Hanack, and T. N. Lomova, Macroheterocycles **3**, 63 (2010). https://doi.org/10.6060/mhc2010.1.63
33. E. N. Ovchenkova, N. G. Bichan, and T. N. Lomova, Tetrahedron **71**, 6659 (2015). https://doi.org/10.1016/j.tet.2015.07.054
34. T. N. Lomova and B. D. Berezin, Russ. J. Coord. Chem. **27**, 85 (2001). https://doi.org/10.1023/A:1009523115380
35. M. E. Klyueva, *Doctoral Sci. (Chem.) Dissertation*, Moscow, 2006.
36. P. Turner and M. J. Gunter, Inorg. Chem. **33**, 1406 (1994). https://doi.org/10.1021/ic00085a032
37. A. Ikezaki and M. Nakamura, J. Porphyrins Phthalocyanines **20**, 318 (2016).
38. A. Ikezaki and M. Nakamura, Chem. Lett. **34**, 1046 (2005). https://doi.org/10.1246/cl.2005.1046
39. G. R. Fulmer, A. J. M. Miller, N. H. Sherden, et al., Organometallics **29**, 2176 (2010). https://doi.org/10.1021/om100106e
40. E. N. Ovchenkova, N. G. Bichan, A. V. Lyubimtsev, et al., Russ. J. Gen. Chem. **88**, 1657 (2018). https://doi.org/10.1134/S1070363218080170
41. K. A. Askarov, B. D. Berezin, R. P. Evstigneeva, et al., *Porphyrins: Structure, Properties, Synthesis*, Ed. by N. S. Enikolopyan (Nauka, Moscow, 1985) [in Russian].
42. T. Lomova, Appl. Organomet. Chem. **35**, e6254 (2021). https://doi.org/10.1002/aoc.6254
43. E. N. Ovchenkova, N. G. Bichan, and T. N. Lomova, Russ. J. Phys. Chem. **93**, 236 (2019). https://doi.org/10.1134/S0036024419010217
44. T. N. Lomova, S. V. Zaitseva, O. V. Molodkina, et al., Russ. J. Coord. Chem. **25**, 397 (1999).
45. K. M. Kadish, L. A. Bottomley, and D. Beroiz, Inorg. Chem. **17**, 1124 (1978). https://doi.org/10.1021/ic50183a006
46. F. A. Walker, J. Am. Chem. Soc. **95**, 1150 (1973). https://doi.org/10.1021/ja00785a025
47. X. Q. Lin, B. Boisselier-Cocolios, and K. M. Kadish, Inorg. Chem. **25**, 3242 (1986). https://doi.org/10.1021/ic00238a030
48. E. N. Ovchenkova, N. G. Bichan, A. S. Semeikin, et al., Macroheterocycles **11**, 79 (2018). https://doi.org/10.6060/mhc170301o

Translated by Z. Svitanko